

Synthesis, Structural, Morphological Properties of Cobalt-Aluminum Nano-Composite

N. M. Deraz^{1,2,*}, Moustafa M. G. Fouda^{1,3}

¹ Chemistry Department, College of Science, King Saud University, P.O. Box 2455, Riyadh 11451, Saudi Arabia.

² Physical Chemistry Department, Laboratory of Surface Chemistry and Catalysis, National Research Center, Dokki, Cairo, Egypt.

³ Textile Research Division, National Research Center, Dokki, Cairo, Egypt, P.O. Box 12622, Giza 12522, Egypt.

*E-mail: nmderaz@yahoo.com

Received: 12 December 2012 / *Accepted:* 8 January 2013 / *Published:* 1 February 2013

Co/Al nano-composite was prepared by combustion method. The structural properties of the final products such as crystallite size, lattice constant, unit cell volume, X-ray density, cation distribution of were determined by X-ray diffraction (XRD) and infrared (IR) techniques. The microstructure and the surface concentration of elements were studied by Scanning electron micrographs (SEM) and Energy dispersive X-ray (EDX) techniques. The results revealed that this method brought about the formation of well crystalline cobalt aluminates (CoAl_2O_4) with spinel structure. The increase in the cobalt content resulted in formation of $\text{CoO}/\text{CoAl}_2\text{O}_4$ nano-composite with subsequent increase in the crystallinity of CoAl_2O_4 phase. However, the as synthesized powders were spongy and fragile.

Keywords: XRD; SEM, EDX; $\text{CoO}/\text{Al}_2\text{O}_3$ nano-composite.

1. INTRODUCTION

Aluminates are chemical compounds consisting of ceramic materials based upon aluminum oxide as principal component. The materials based on the aluminates are potential candidates for modern technological applications due to their unique potential application in high density magnetic recording, microwave devices, magnetic fluids, heterogeneous catalysis and absorbent materials [1, 2]. Most of the ceramic dyeing materials used in pigment industries are of transition metal oxides with the spinel structure having high surface area, thermal stability and chemical resistance [3]. Cobalt

aluminates, CoAl_2O_4 , is regarded as an important candidate of the normal spinel aluminates family with aluminum in octahedral sites and cobalt in tetrahedral ones [4].

CoAl_2O_4 powders are often prepared by the traditional method via the heat treatment for a mixture of the corresponding oxides [4]. Conventional preparation of aluminates requires a number of stages, including homogenization of the powder precursors, compaction of the reactants, and finally prolonged heat treatment at considerably elevated temperatures. Several methods are conventionally used for the synthesis of nano-sized CoAl_2O_4 spinel such as chemical co-precipitation, sol-gel, polymeric precursor and hydrothermal treatment [5-9].

Preparation of spinel materials were prepared by glycine assisted combustion route [10- 12]. This route has the advantage over other low-temperature methods in the sense that, one will get batches of bigger yield in a short time period. Combustion synthesis is a particularly simple, safe and rapid fabrication process, wherein the main advantages are energy and time savings. This quick, straightforward process can be used to synthesize homogeneous, high-purity, crystalline oxide ceramic powders including nano-sized cobalt aluminate powders with a broad range of particle sizes.

In the current study, we aim to prepare $\text{CoO}/\text{Al}_2\text{O}_3$ nano-composite via glycine-assisted combustion method. Another goal for this investigation is the study of the effect of molar ratio for Co and Al on the structural and morphological properties of the prepared $\text{CoO}/\text{Al}_2\text{O}_3$ nan-composite. The techniques employed were XRD, IR, EDX and SEM.

2. EXPERIMENTAL

2.1. Materials

Two samples of $\text{CoO}/\text{Al}_2\text{O}_3$ composite were prepared by mixing calculated proportions of cobalt and aluminum nitrates with a certain amount of glycine. The mixed precursors were concentrated in a porcelain crucible on a hot plate at $350\text{ }^\circ\text{C}$ for 5 minutes. The crystal water was gradually vaporized during heating and when a crucible temperature was reached, a great deal of foams produced and spark appeared at one corner which spread through the mass, yielding a brown voluminous and fluffy product in the container. In our experiment, the ratio of the glycine: aluminum: cobalt nitrates were 4: 1: (1, 2) for S1 and S2 samples, respectively. The chemicals employed in the present work were of analytical grade supplied by Fluke Company.

2.2. Techniques

An X-ray measurement of various mixed solids was carried out using a BRUKER D8 advance diffractometer (Germany). The patterns were run with Cu K_α radiation at 40 kV and 40 mA with scanning speed in 2θ of $2\text{ }^\circ\text{ min}^{-1}$.

The crystallite size of both CoO and CoAl_2O_4 present in the investigated solids was based on X-ray diffraction line broadening and calculated by using Scherrer equation [13].

$$d = \frac{B\lambda}{\beta \cos \theta} \quad (1)$$

where d is the average crystallite size of the phase under investigation, B is the Scherrer constant (0.89), λ is the wave length of X-ray beam used, β is the full-width half maximum (FWHM) of diffraction and θ is the Bragg's angle.

Scanning electron micrographs (SEM) were recorded on SEM-JEOL JAX-840A electron microanalyzer (Japan). The samples were dispersed in ethanol and then treated ultrasonically in order to disperse individual particles over a gold grid.

Energy dispersive X-ray (EDX) analysis was carried out on Hitachi S-800 electron microscope with an attached keveX Delta system. The parameters were as follows: accelerating voltage 10, 15 and 20 kV, accumulation time 100s, window width 8 μm . The surface molar composition was determined by the Asa method, Zaf-correction, Gaussian approximation.

3. RESULTS AND DISCUSSION

3.1. Structural analysis

The XRD patterns for S1 and S2 samples containing different molar ratios of cobalt and aluminum are given in Fig. 1.

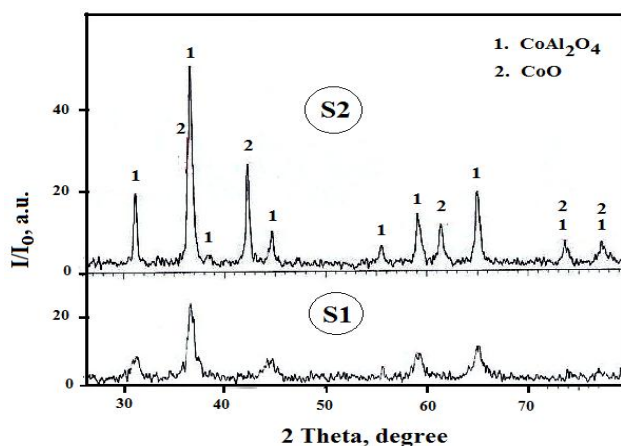


Figure 1. XRD pattern for the S1 and S2 samples.

Examination of this figure revealed that: (i) The S1 sample consisted entirely of cubic spinel cobalt aluminates, CoAl₂O₄, as a single phase. One cannot ignore the presence of amorphous cobalt oxide because the Co/Al ratio equals to one depending upon the stoichiometry of the previous ratio is

0.5. (ii) The S2 sample consisted of CoO and CoAl₂O₄ phases. The major phase in this sample is moderate crystalline CoAl₂O₄ nano- particles. However, the element cobalt has long been known to have two stable crystal line structures: close-packed hexagonal (hcp) and face-centered cubic (fcc). Both phases can exist at room temperature. The fcc structure is thermodynamically preferred above 450 °C and the hcp phase is favored at lower temperatures. For small particles, however, the fcc structure appears to be preferred even below room temperature [14]. But the cobalt species settle in the fcc crystal structure due to the presence of the aluminum matrix [15]. (iii) In the XRD pattern for the S2 sample, the diffraction peaks of both CoO and CoAl₂O₄ phases gradually become sharp and their intensities increase as the cobalt content increases, revealing an increase of the size of these phases.

3.2. The size control of CoAl₂O₄ nano- crystals

In this study, we can control the size of CoAl₂O₄ nano-crystals by tuning the molar ratio of CoO to Al₂O₃. In other words, judicious adjustment of the metal precursor- to-fuel ratio can control the size of nano- crystals. Indeed, the change in the ratio of glycine to metal nitrates by increasing the cobalt content resulted in an increase in the crystallite size (d) of CoAl₂O₄ nano- particles as shown in Table 1. Also, Table 1 displays the lattice constant (a), unit cell volume (V) and X-ray density (D_x) of CoO and CoAl₂O₄ nano- particles depending upon the data of X-ray.

Table 1. Some structural parameters for the crystalline phases involved in the Co/Al nano- composites.

Samples	CoAl ₂ O ₄				CoO			
	d (nm)	a (nm)	V (nm ³)	D _x (g/cm ³)	d (nm)	a (nm)	V (nm ³)	D _x (g/cm ³)
S1	22	0.8086	0.5287	4.4430	-	-	-	-
S2	26	0.8104	0.5322	4.4140	37	0.4266	0.7765	6.4080

As the amount of cobalt species increases as the values of crystallite size, lattice constant and unit cell volume of CoAl₂O₄ nano-crystals increase. Opposite behavior was observed for X-ray density (D_x) of CoAl₂O₄ nano- particles. So, the incorporation of CoO ions in the lattice of CoAl₂O₄ brought about an increase in the lattice constant of CoAl₂O₄ particles with subsequent expansion in their lattices depending upon the difference in the ionic radii between Co and Al species. On the other hand, the increase in the peak height of CoAl₂O₄ phase in the S2 sample could be attributed to the solid state reaction between CoO and Al₂O₃ yielding cobalt- aluminum compound. The decrease in the density due to the increase in cobalt content could be ascribed to the reduction of oxygen vacancies which play a predominant role in accelerating densification i.e. the decrease in oxygen ion diffusion would retard the densification.

3.3. Formation of spinel CoAl_2O_4 compound

The spinel-type CoAl_2O_4 compound can be prepared by the conventional standard method via solid state reaction between CoO and Al_2O_3 depending upon the thermal diffusion for the cations of these oxides [16]. Various factors such as precursor compounds, preparation method and preparation conditions affect the thermal diffusion of Co and Al cations through the early cobalt aluminates film which covers the surfaces of grains of reacting oxides and acts as energy barrier. The conventional standard method often leads to two disadvantages: (i) the milling and grinding, normally employed to obtain a mixture (Co and Al oxides), can hardly obtain a micro-homogeneous phase structure and introduces contaminates, which have a detrimental effect on the material properties, and (ii) the mechanically-ground mixture requires prolonged calcinations at high temperatures (>1200 °C), which often leads to materials with low surface area and undesirable crystallite growth [1]. So, this method is not adequate for many advanced applications. Recently, the previous materials were produced by different methods such as sol-gel, co-precipitation, hydrothermal, and thermal decomposition of organic precursors [17-20].

Among these techniques, the glycine assisted combustion route which attracted the attention of the scientists of nano-science to obtain the homogeneity of the metal ion distribution on the atomic level depending upon the formation of complex materials that pyrolyze at a low temperature and form the desired oxide compositions. This method prevents partial segregation of metal compounds [16]. Deraz reported that the glycine assisted combustion method is useful for providing an alternative of low cost mass production of various spinel ferrite materials [21, 22].

The counter-diffusion of Co^{2+} and Al^{3+} through a relatively rigid aluminate film led to the formation of CoAl_2O_4 particles. We speculate that the diffusing ions might be Co^{2+} including Co^{3+} on the basis of detecting Co^{2+} in the interface. In addition, following reactions indicate that Al_2O_3 decomposes to 2Al^{2+} and oxygen gas at Al_2O_3 - interface. Moreover, oxygen moves through the reacted area to be added to the CoO interface and form spinel by reacting with aluminum ions:

At Al_2O_3 interface:



At CoO interface:



The IR transmission spectra for the samples S1 and S2 were recorded in the range of 1000 - 350 cm^{-1} as shown in Fig. 2. It can see from this figure that the investigated method led to formation of spinel CoAl_2O_4 compound.

In the range of 1000 - 350 cm^{-1} , the IR bands for the as prepared solids are usually assigned to vibration of ions in the crystal lattice. Two main metal- oxygen bands are seen in the IR spectra of all spinels [23], namely tetrahedral (A-sites) and octahedral (B-sites) according to the geometrical configuration of nearest neighbors. The highest band ν_1 , generally observed around 600cm^{-1} , corresponds to intrinsic stretching vibrations of metal at the tetrahedral site, whereas the ν_2 lowest

band, usually observed around 400 cm^{-1} , is assigned to octahedral- metal stretching. In inverse aluminates such as cobalt aluminates, the ν_1 and ν_2 bands are due to $\text{Al}^{3+}\text{-O}^{2-}$ complexes present at A- and B-sites. The Co^{2+} ions occupy mainly the octahedral sites and fraction goes into tetrahedral sites [22]. This would explain the existence of a weak shoulder, ν_1' around ν_1 band. It can be seen from Fig. 2 that: (i) the spectra of mixed solids consisted of ν_1 and ν_2 at 665 ± 3 and $565\pm 3\text{ cm}^{-1}$, respectively. The shoulder ν_1' in A- sites appears at 750 cm^{-1} . (ii) The difference in positions of the absorption bands ν_1 and ν_2 is referred to change the formation of cobalt aluminates by changing the cobalt content because the positions of the bands ν_1 and ν_2 depend strongly on the method and conditions of preparation. However, the increase in the Co content resulted in an increase in the intensities of both the bands ν_1 and ν_2 . These observations suggested that the formation of spinel cobalt aluminates increases as the cobalt content increases.

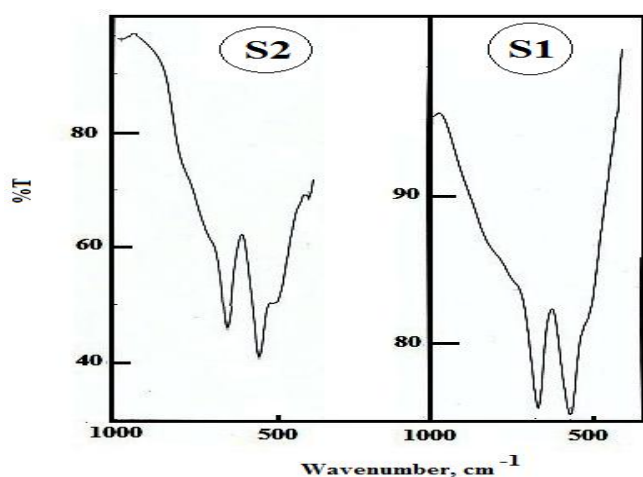


Figure 2. IR spectra for the S1 and S2 samples.

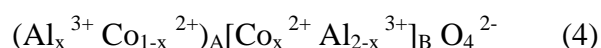
3.4. Cation distribution

The intensities of the (2 2 0) and (4 4 0) planes are more sensitive to the cations on tetrahedral, and octahedral, respectively [22]. Indeed, the Co^{2+} and Al^{3+} ions have a strong preference to occupy A and B sites, respectively [4]. Table 2 shows the observed intensities of the above planes.

Table 2. The intensity values of some hkl planes for the as prepared cobalt aluminate.

Samples	Peak height (a. u.)		
	I_{220}	I_{440}	I_{220}/I_{440}
S1	8.6	10.8	0.796
S2	19.1	19.5	0.979

It can be observed that the intensity of the (2 2 0) and (4 4 0) planes increases as the content of cobalt increase. This infers that the Co^{2+} ions have preferentially occupied both the A and B sites. But, the amount of cobalt species at A site is greater than that at B site [4]. This speculation confirms from the maximum increase in the intensity of both (2 2 0) and (4 4 0) planes which attained 122.1% and 80.6%, respectively. This result might show that the solubility of CoO at A sites is greater than that at B sites involved in the cobalt aluminates lattice. However, the substitution of some Al^{3+} ions by Co^{2+} ions at B site resulted in migration of these ions (Al^{3+}) from B site to A site. In other words, the increase in the cobalt content brought about an increase in the number of Co^{2+} ions on A site with subsequent increase in the crystallite size, lattice constant and unit cell volume of cobalt- aluminum compound. On the basis of the above data, the inverted spinel structure can be assigned in the synthesized materials having the formula CoAl_2O_4 can be expressed as:



The parameter of inversion, x , is equal 0 for inverse spinel and to 1 when the spinel is normal.

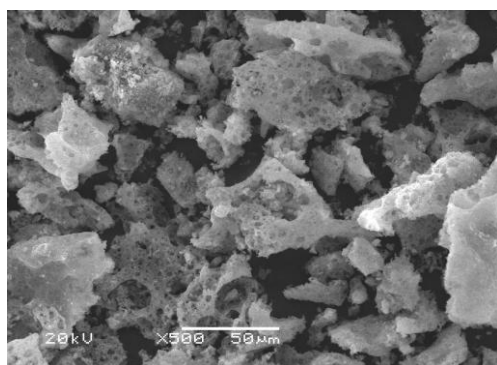
From the data of X-ray, the distance between the reacting ions (L_A and L_B), ionic radii (r_A , r_B) and bond lengths (A–O and B–O) on tetrahedral (A) sites and octahedral (B) sites of CoAl_2O_4 crystallites were summarized in Table 3. This table showed that the increase in the content of cobalt resulted in an increase in the calculated values of L_A , L_B , r_A , r_B , A–O and B–O of CoAl_2O_4 crystallites. These findings confirm the increase in the crystallite size, lattice constant and unit cell volume of CoAl_2O_4 nano- particles.

Table 3. The of L_A , L_B , A-O, B-O, r_A and r_B for the as prepared cobalt aluminates.

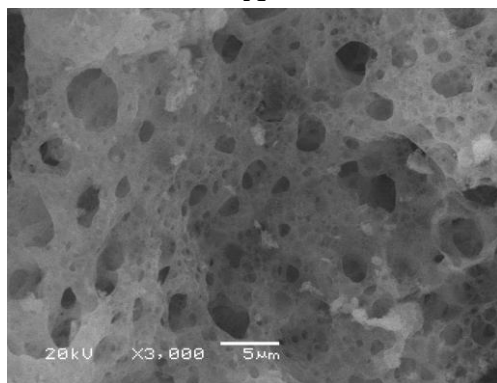
Samples	L_A (nm)	L_B (nm)	A-O (nm)	B-O (nm)	r_A (nm)	r_B (nm)
S1	0.3501	0.2859	0.1821	0.2053	0.0471	0.0704
S2	0.3509	0.2865	0.1825	0.2058	0.0475	0.0708

3.5. The morphology investigation

Figs. 3 and 4 show the SEM images for S1 and S2 samples with different magnifications. We can see from these figures that the as synthesized samples are spongy and fragile materials. However, voids and pores are observed in the as prepared samples. These findings could be attributed to the release of large amounts of gases during combustion process due to decomposition of the glycine and Co and Al nitrates. In addition, the porosity of the S2 sample is greater than that of the S1 sample due to the large amount of the released gases. In fact, the X-ray density of the S2 sample is lower than that of the S1 samples. It can be seen from Figs. 2 and 3 that the agglomeration of the particles involved in the S1 sample is greater than that in the S2 samples. This indicates that the increase in the Co content hinders the aggregation of the particles involved in the Co/Al nano-composites.

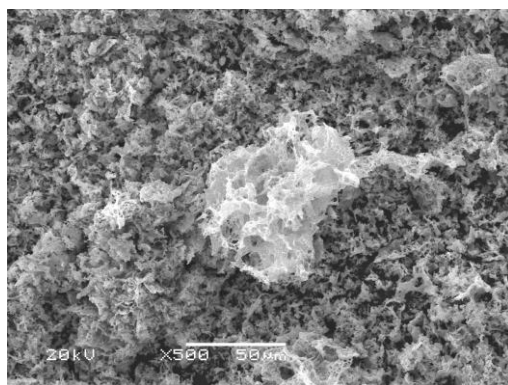


A

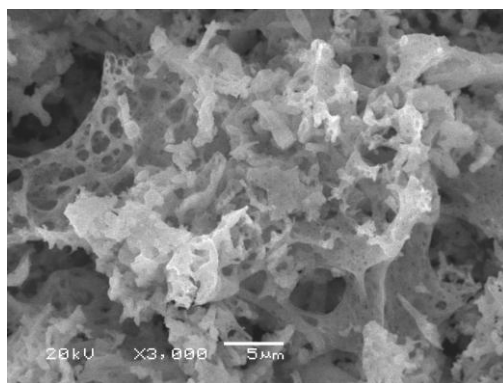


B

Figure 3. SEM images for the S1 sample.



A



B

Figure 4. SEM images for the S2 sample.

3.6. Homogeneity of the as prepared samples

Energy dispersive X-ray (EDX) analysis over different areas on surface of the as prepared samples at 20 keV was carried out. The relative atomic abundance of O, Co and Al species present in the surface layers of The S1 and S2 samples are given in Tables 4 and 5, respectively. These tables showed that the surface concentrations of O, Co and Al species at 20 keV on different areas over the surface of specimens studied are much closed to each other. This indicates the homogeneous distribution of O, Co and Al species in the investigated samples. Thus, the combustion route resulted in production of homogeneously distributed materials.

Table 4. The atomic abundance of elements measured at 20 keV and different areas over the S1 sample.

Elements	Area	Area	Area	Area
	1	2	3	4
O	26.68	28.16	27.98	25.00
Co	62.35	57.83	58,39	67.48
Al	10.97	14.01	13.63	7.51

Table 5. The atomic abundance of elements measured at 20 keV and different areas over the S1 sample.

Elements	Area	Area	Area	Area
	1	2	3	4
O	24.69	24.59	24.93	24.76
Co	68.44	68.75	67.71	68.23
Al	6.87	6.66	7.36	7.01

3.7. The elements gradient

EDX investigation at 5, 10, 15 and 20 keV showed the concentrations of Co, Al and oxygen species from the uppermost surface to the bulk layers for the two investigated samples as shown Figs. 4 and 5.

The obtained data was summarized in Tables 6 and 7.

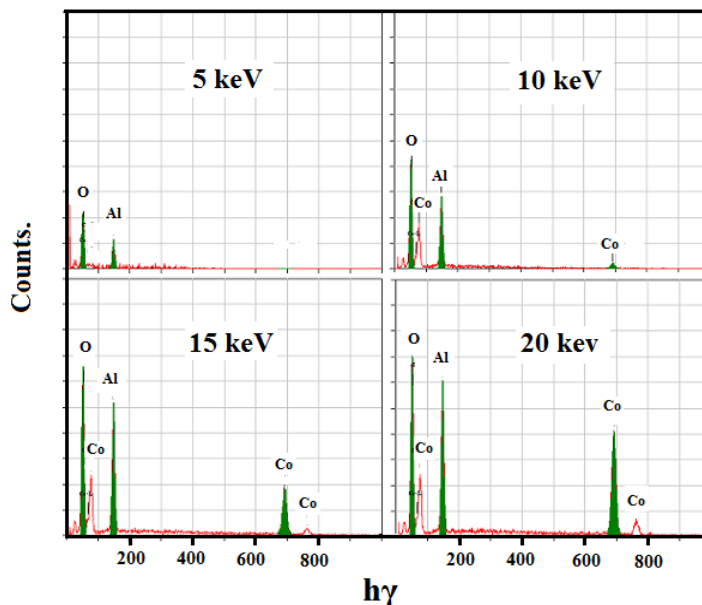


Figure 5. EDX pattern for the S1 sample at different applied voltages.

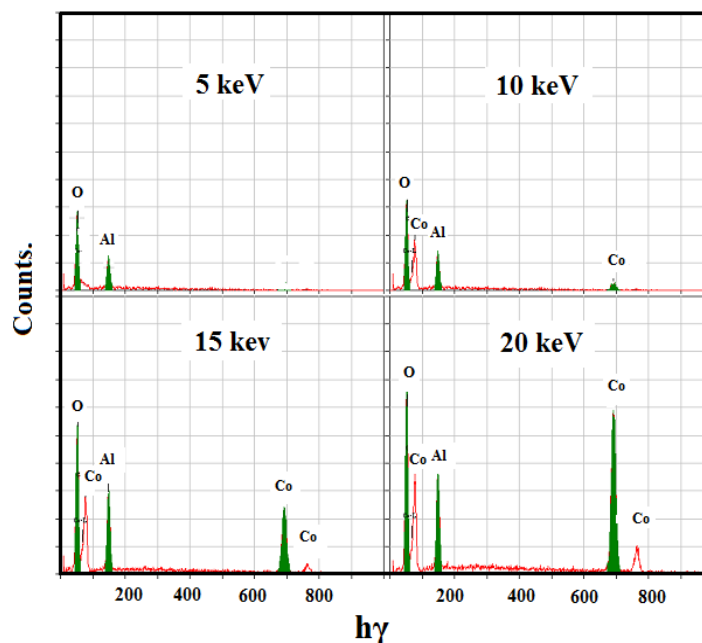


Figure 6. EDX pattern for the S2 sample at different applied voltages.

Inspection of Tables 6 and 7 revealed that: (i) the surface concentrations of Al and oxygen species for the S1 and S2 samples decrease as the applied voltage increases from 5 to 20 keV. This indicates that the uppermost surface layer of the two prepared samples is O- and Al-rich layer. (ii) The absence of the Co species at uppermost surface layer of the two prepared samples. Indeed, the surface concentrations of Co species at 5 keV are zero for the S1 and S2 samples. The increase in the applied voltage above the previous limit (5 keV) showed that the surface concentrations of Co species increase from the uppermost surface layer to the bulk of the as prepared materials. These findings suggest a

possible redistribution for the elements involved in the as synthesized composites with subsequent unique properties of these composites.

Table 6. The atomic abundance of elements measured at different voltages over the same area for the S1 sample.

Elements	Atomic abundance (%)			
	5 keV	10 keV	15 keV	20 keV
O	47.07	35.34	29.40	27.65
Co	00.00	35.88	54.03	59.39
Al	52.93	28.78	16.57	12.96

Table 7. The atomic abundance of elements measured at different voltages over the same area for the S1 sample.

Elements	Atomic abundance (%)			
	5 keV	10 keV	15 keV	20 keV
O	47.07	29.55	25.70	24.27
Co	00.00	53.59	65.34	69.73
Al	52.93	16.86	8.96	6.00

4. CONCLUSIONS

Glycine- assisted combustion method was used to synthesis of Co- Al nano- composites. Changing of the molar ratio between Co and Al species led to different changes in the structural and morphological properties of the as prepared solids. In this study, the combustion route resulted in the production of spinel CoAl_2O_4 nano- particles. The increase in the cobalt content resulted in an increase in the crystallite size, lattice constant and unit cell volume of the produced cobalt aluminates. Opposite behavior was observed in the value of the X-ray density. The images of SEM showed that the sample containing the high amount of cobalt has a significant porosity. The obtained samples have a

homogenously distributed species in the whole mass prepared. The surface concentrations of Co, Al and oxygen species for the S1 and S2 samples change by changing the molar ratio between Co and Al species.

ACKNOWLEDGEMENT

The authors extend their appreciation to the Deanship of Scientific Research at King Saud University for funding this work through research group no RGP- VPP-201.

References

1. S. Bid and S.K. Pradan, *Mater. Chem. Phys.*, 82 27 (2003).
2. R.E. Ayala and D.W. Marsh, *Ind. Chem. Res.*, 30(1991) 55.
3. N. Ouahdi, S. Guillemet J.J. Demai, B. Durand L. Er. Rakho, R.Moussa and A.Samdi, *Mater. Lett.*, 95(2005) 334.
4. M. Zayat, D. Levy, *Chem. Mater.* 12 (2000) 2763.
5. Bolt, P. H., Habraken, F. H. P. M and Geus, J. W., *J. Solid. State Chem.*, 135(1998)59.
6. S. Chokkaram, R. Srinivasan, D. R. Milburn, B. H. Davis, *J. Mol. Catal. A: Chem.*, 121(1997)157.
7. U. L. Stangar, B. Orel, M. Krajnc, R. C. Korosec, P. Bukovec, *Materiali in Thechnologije*, 36(2002)387..
8. W. S. Cho, M. Kakihana, *J. Alloys Compd.* 287(999)87.
9. Z. Z. Chen, E. W. Shi, W. J. Li, Y. Q. Zheng, J. Y. Zhuang, B. Xiao, L. A. Tang, *Mater. Sci. Eng. B*, 107(2004)217.
10. N. M. Deraz, A. Alarifi, *Int. J. Electrochem. Sci.*, 7(2012) 3798.
11. N. M. Deraz, A. Alarifi, *Int. J. Electrochem. Sci.*, 7(2012) 3809.
12. N. M. Deraz, A. Alarifi, *Int. J. Electrochem. Sci.*, 7(2012) 5534.
13. B.D. Cullity, *Elements of X-ray Diffraction*, Addison-Wesly Publishing Co. Inc. 1976 (Chapter 14).
14. Power diffraction file PDF-2 database sets (1994) pp. 1-44.
15. P Anil Kumar, Subarna Mitra, Kalyan Mandal, *Indian J. Pure and Appl. Phys.*, 45(2007)21.
16. Cuiyan Wang, Shaomin Liu, Lihong Liu, Xuan Bai, *Mater. Chem. Phys.*, 96 (2006) 361.
17. L. Ji, J. Lin, K.L. Tan, H.C. Zeng, *Chem. Mater.*, 12 (2000) 931.
18. U. Chellam, Z.P. Xu, H.C. Zeng, *Chem. Mater.*, 12 (2000) 650.
19. E.L. Uzunova, I.G. Mitov, D.G. Klissurski, *Bull. Chem. Soc. Jpn.* 70 (1997) 1985.
20. C. Wang, X. Bai, S. Liu, L. Liu, *J. Mater. Sci.* 39 (2004) 6191.
21. N. M. Deraz, *Ceramics International*, 38 (2012) 511.
22. N. M. Deraz, *Int. J. Electrochem. Sci.*, 7(2012) 4596.
23. R. D. Waldron, *Phys. Rev.*, 99 (1955) 1727.